Journal of Hydrology: Regional Studies 3 (2015) 494–508

Contents lists available at ScienceDirect

Journal of Hydrology: Regional Studies

journal homepage: www.elsevier.com/locate/ejrh

Causes of interannual to decadal variability of Gila River streamflow over the past century

M.A. Pascolini-Campbell[a,*], Richard Seager[b], David S. Gutzler[c], Benjamin I. Cook[d], Daniel Griffin[e,f]

[a] Department of Earth and Environmental Sciences, Columbia University, New York, USA
[b] Lamont Doherty Earth Observatory of Columbia University, Palisades, NY, USA
[c] University of New Mexico, Albuquerque, NM, USA
[d] NASA Goddard Institute for Space Studies, New York, USA
[e] Woods Hole Oceanographic Institution, Woods Hole, USA
[f] University of Minnesota, Minnesota, USA

ARTICLE INFO

Article history:
Received 14 June 2014
Received in revised form 17 December 2014
Accepted 22 February 2015
Available online 1 May 2015

Keywords:
Streamflow decadal variability
Drought
Pluvials
Treering
Teleconnections
North American Monsoon

ABSTRACT

Study region: The Gila River, New Mexico, is characterized by two peaks in streamflow: one in the winter–spring (December–May), and summer (August–September). The region is influenced both by Pacific SST variability as well as the North American Monsoon.

Study focus: The mechanisms responsible for the variability of the winter–spring and summer streamflow peaks are investigated by correlation of streamflow with precipitation and sea surface temperature for 1928–2012. Decadal variability in the flow record is examined for a longer term perspective on Gila River streamflow using tree ring-based reconstructions of the Palmer Drought Severity Index (PDSI) and the Standardized Precipitation Index (SPI).

New hydrological insights for the region: Results indicate a strong influence of winter–spring precipitation and Pacific SST anomalies on the winter–spring streamflow, with El Niño conditions in the Pacific causing increased precipitation and streamflow. Decadal Pacific variability helps explain the transition from high winter flow in the late 20th century to lower flows in the most recent decade. The summer streamflow has a somewhat weaker correlation with precipitation and Pacific SST than the winter–spring streamflow. Its variability is more likely influenced by local North American Monsoon precipitation variability. PDSI and SPI reconstructions indicate much more severe and extended periods of droughts and pluvials in past centuries as well as periods of concurrent winter and summer drought.

* Corresponding author. Tel.: +1 347346009.

http://dx.doi.org/10.1016/j.ejrh.2015.02.013

1. Introduction

The Gila River flows approximately 600 miles west across Arizona, from its headwaters in New Mexico to join the Colorado River just above its mouth. The Gila River receives water from both extratropical winter storms and the North American Monsoon, producing a complex hydrograph with spring and summer peak flows (Gutzler, 2013). The Gila River has been gaged since 1928 and its historical flows show considerable interannual to decadal variability (ibid.). Precipitation and streamflows of other rivers in the Southwest have been shown to be affected by various mechanisms, including responses to Pacific and Atlantic sea surface temperature (SST) anomalies (Gutzler et al., 2002; Sheppard et al., 2002; McCabe et al., 2004). In addition to the influences of climate variability, aridity in the Southwest United States is projected to intensify with global warming (Seager et al., 2007, 2014) and this will have implications for precipitation and streamflow in the region. Understanding these varying influences on streamflow is vital for producing reliable projections of future streamflows and water resources in the coming decades.

The Gila River is a vital source of water for multiple groups in New Mexico and Arizona including farmers, industries, and local communities including the Gila River Indian Community. It supplies water to Catron, Grant, Hidalgo and Luna Counties, New Mexico, for varied purposes including agriculture (which accounts for 86% of water consumption in the state (Liverman and Merideth, 2002)), commercial use, industry, mining and power extraction. The Gila River is also the subject of an ongoing debate on planning for water use in New Mexico as allowed under the Arizona Water Settlements Act (AWSA). The social importance of the river motivates the need for improved scientific understanding of the mechanisms responsible for its flow.

Here we present the first comprehensive study of historical Gila River flow variability. Since the river is fed by (1) snowmelt in the spring and (2) the North American Monsoon in the summer, attention must focus on both winter and summer season climate variability. Many previous studies have demonstrated the connection between Southwest precipitation during the winter and Pacific Ocean SST anomalies (Molles and Dahm, 1990; Redmond and Koch, 1991; Kahya and Dracup, 1993, 1994; Cayan et al., 1999; Seager et al., 2005a). This connection is primarily due to the El Niño-Southern Oscillation (ENSO) (Cayan et al., 1999), a coupled atmosphere–ocean phenomenon with equatorial Pacific SST varying at the 2–7 years timescale and being strongest during the winter (December–January–February (DJF)) season (e.g. (Trenberth, 1997)). The Pacific Decadal Oscillation (PDO) has also been found to influence hydroclimate in the region (Barlow et al., 2001). Those studies found that winters of warm SST anomalies (El Niño events) precede higher than average spring streamflow and precipitation in southwest North America, and periods of cold SST anomalies (La Niña events) tended to go along with low precipitation and streamflow (Cayan et al., 1999). Focusing on precipitation variability, modeling studies have also indicated the importance of Pacific SST anomalies in generating persistent, multiyear, droughts and pluvials in North America (Schubert et al., 2004; Seager et al., 2005b), and multidecadal precipitation variability (Seager et al., 2014).

From Mexico into the southwestern U.S., the North American Monsoon brings a summer (July–August–September (JAS)) peak in rainfall (Adams and Comrie, 1997; Barlow et al., 1998) and Monsoon variability presumably can also drive streamflow variability, including of the Gila. Modeling studies have indicated that greenhouse gas (GHG) warming could delay both Monsoon onset and retreat (Seth et al., 2013; Cook and Seager, 2013) though changes in the Monsoon by region have not yet been closely examined. In addition, the role of increased temperature and potential evapotranspiration rates is predicted to have an impact on the hydrology of the region, adding a further dimension to streamflow change in the future (Hurd and Coonrod, 2008; Gutzler, 2013).

This study will investigate historical variability of Gila River flow, the nature of the double peaked hydrograph, and in particular the association of flow to SST anomalies in the Pacific and Atlantic Oceans. Key questions addressed will include: (1) precipitation variability in which months best explains the variability of the two peak streamflows?, (2) how are precipitation over the basin and streamflow related to SST anomalies?, (3) what is the relationship of flow variability to ENSO?, and (4) what is the nature and cause of the decadal variability of Gila River flow since 1928. Future climate change impacts on Gila River flow are not examined here (but see (Gutzler, 2013)). Instead we use observations

to explain the past flow variability as one necessary step to understanding its potential present and future predictability.

2. Data and methodology

To investigate streamflow and climate variability four observational datasets for the time period of 1928–2012 are used. This time span is used as the base period from which climate anomalies are calculated. For streamflow we use mean daily values for the upper Gila River from United States Geological Survey (USGS) Gage Data (in units of cubic meters per second (c.m.s.)) (USGS gage 09430500) (data last accessed 12/10/2014 online at http://waterdata.usgs.gov/nwis/uv?siteno=09430500) (Gila River and position of USGS gage shown in Fig. 1). For precipitation we use two datasets: the first is from the Global Precipitation Climatology Center (GPCC) (in units of mm/month on a $0.5^\circ \times 0.5^\circ$ global grid) which is used for generating data over North America for 1928–2010. The second precipitation dataset used is from the Parameter Regression on Independent Slopes Model (PRISM; in units of mm/month on a 4 km grid), which uses a well-verified, terrain-sensitive algorithm to interpolate between available stations over the period 1895–present (Daly et al., 2008). To focus on watershed specific variability, PRISM data was extracted for the Upper Gila Basin (U.S.G.S. Hydrologic Unit Code 150400) using the Westmap Internet tool (http://www.cefa.dri.edu/Westmap/). The interpolation between stations in the PRISM data is sensitive to elevation changes, which is important given the varying topography of the study region. For SST, ERSST V3 reanalysis data (in units of degrees Celsius on a 2°x2° global grid) are used (Smith et al., 2008). A reconstruction of the Palmer Drought Severity Index (PDSI) for the United States, based on tree ring data within the North American Drought Atlas (NADAV2a), is used since 1530 A.D. (Cook et al., 2004, 2007, 2010). Season-specific moisture variability in the pre-instrumental era was assessed with tree-ring reconstructions to create the Standardized Precipitation Index (SPI) for the 7-month season ending in April and the 3-month season ending in August for 1530–2008 (Griffin et al., 2013). For evapotranspiration, precipitation and temperature output is used from the Global Land Data Assimilation System (GLDAS) Common Land Model (CLM) (1979–2000)

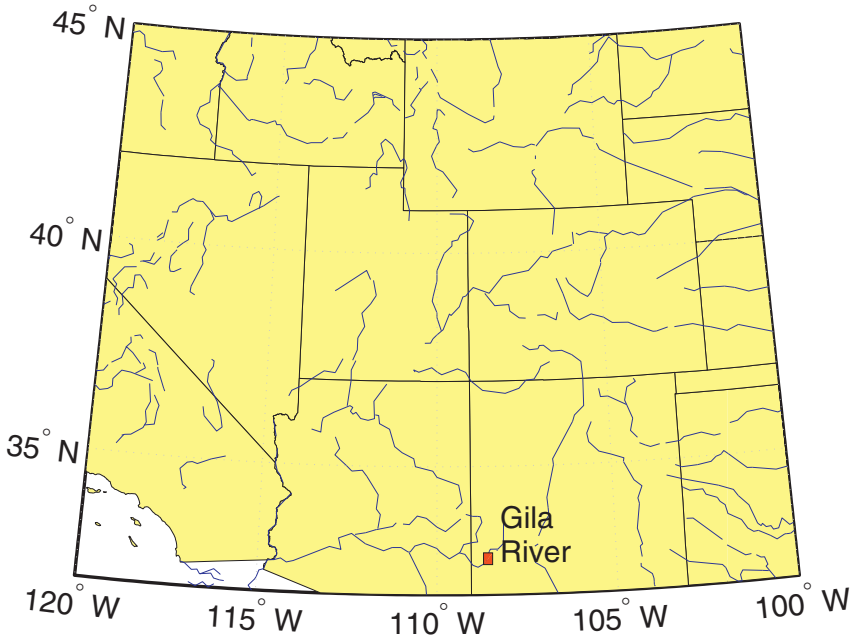

Fig. 1. Map of the United States southwest and location of the Gila River. Red square indicates the location of USGS gage 09430500 located at 108°W and 33°N

(Rodell et al., 2004), the Variable Infiltration Capacity (VIC) hydrological model (1929–2003) (Liang, 1994) as well as NCEP-NCAR CDAS-1 Reanalysis data (1948–2012) (Kalnay et al., 1996) ((in units of $kg/m^2/s$ for precipitation and evapotranspiration, and degrees Celsius for temperature, on a $1^\circ x1^\circ$ global grid). The Variable Infiltration Capacity (VIC) hydrological model is also used for evapotranspiration, precipitation and temperature from 1929–2003 (Liang, 1994).The GPCC precipitation, SST and PDSI datasets are available online at the International Research Institute Institute for Climate and Society (IRI) data library (http://iridl.ldeo.columbia.edu/).

To investigate precipitation variations over the Gila River Basin, a time series is constructed from the PRISM data for the Upper Gila Hydrological Unit. Regions affected by the North American Monsoon have been found to contain large degrees of spatial heterogeneity in rainfall and temperature trends, related to the spatially varying nature of convective cloud activity (Gebremichael et al., 2007), making it important to examine links between Gila River flow and precipitation on the scale of the basin itself. For example stronger correlation between precipitation and streamflow was found to exist when using the PRISM Upper Gila Hydrological Unit Precipitation compared with a rectangular box containing the Gila River catchment upstream of the gage (spanning 108.5°W to 111.5°W and 31.5°N to 33.5°N). Pacific Ocean SST variability related to ENSO is investigated using the Niño-4 index, which is the SST anomaly averaged over the area bound by 5°N to 5°S and 150°W to 160°E. The Niño-4 index is used rather than the Niño-3.4 index due to the greater correlation of Gila streamflow and precipitation with the former index. For this reason warm and cold events in the Niño-4 region are considered to represent ENSO variability. All the events classified as El Niño years using Niño-4 are also found to be consistent with the Niño-3.4 classification (http://www.cpc.ncep.noaa.gov/). Composites of precipitation over North America corresponding to cold and warm events in the Niño-4 region are also created. Warm (cold) events are identified as those in which the value of the Niño-4 index for DJF season has an anomaly greater (less) than 0.5°C.

A hydrograph for the Gila River is created using streamflow data to determine the magnitude and timing of the dual peaks (as carried out by (Gutzler, 2013)). Following identification of the peak months of streamflow, a cross-correlation with PRISM precipitation is performed to determine for which months the precipitation is best correlated to flow. Although in general streamflow is expected to correlate with precipitation, other factors such as snowmelt, evaporation and soil moisture may impact the strength of correlations making the precipitation influence interesting to investigate (i.e. (Notaro et al., 2010)). The timeseries of streamflow and precipitation for these months were then correlated with SST for 1928–2012 to create maps of correlation coefficients showing which ocean regions have the greatest influence on Gila River precipitation and flow.

High and low spring streamflow events are then investigated. High events are identified by determining years in which the magnitude of DJFMAM streamflow is greater than 85% of the annual mean, and low events when flow is less than 15% of the annual mean for 1928–2012. Composites of GPCC precipitation and SST patterns for the high and low events are created to examine co-existing patterns. GPCC data are used for precipitation in this case as they provide global coverage and can be used to illustrate patterns across the entire North American continent.

Decadal variability is investigated through analysis of the timeseries for 1928–2012. Composites for GPCC precipitation and SST are created for years of persistently high and low flow to determine the nature of the associated climatic patterns. In addition two dendroclimatological time series are analyzed to examine longer term variability in the region using the winter–spring and summer Standardized Precipitation Indices (SPI). Winter–spring SPI was reconstructed from tree-ring chronologies of earlywood width (EW) and summer SPI was reconstructed from tree-ring chronologies of latewood width (LW) that were adjusted to isolate the variability unique to LW (Griffin et al., 2011; Meko and Baisan, 2001). Cross spectral and cross-wavelet coherence analyses indicates that the winter–spring and summer SPI reconstructions are effectively independent at interannual to decadal timescales, or more specifically, at wavelengths less than approximately 32 years. At longer timescales, the reconstructions are essentially coherent and in phase. A greater level of detail is provided in Griffin et al. (2013). PDSI and SPI are also correlated to examine consistency between the different data sets. Although both contain information on precipitation variability, the PDSI and SPI reconstructions do not share the same numerical input data. The SPI reconstruction was developed from novel measurements of tree-ring earlywood width at only a few sites, data that was not available nor included in the PDSI

reconstructions. In contrast, the PDSI reconstruction is developed from a great many chronologies of total ring width. It is likely that data from some of the same trees entered into both reconstructions, but the data is from a different parameter (earlywood width (SPI) vs. total ring width (PDSI)).

3. Results

The box plot (Fig. 2(a)) shows that peak streamflow occurs during the months December–January–February–March–April–May (DJFMAM) and the summer peak occurs during August–September (AS). For these months streamflow reaches monthly mean magnitudes of approximately 5.6 in winter–spring and 2.7 c.m.s. in summer. Fig. 2 also shows timeseries of streamflow

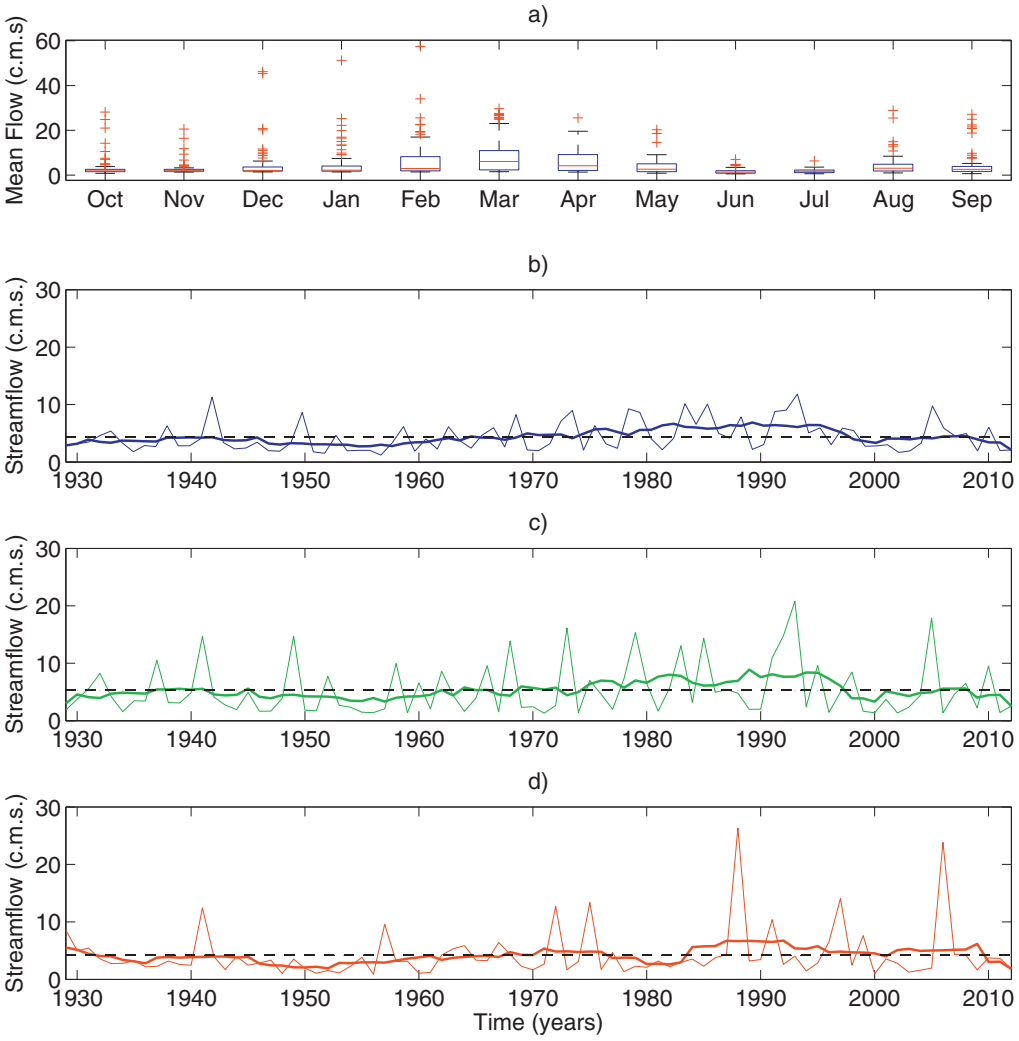

Fig. 2. a) Boxplot of monthly flow over the time period 1928 to 2012. For each boxplot, the central mark is the median, the edges of the box are the 25th and 75th percentiles, the whiskers extend to the most extreme data points not considered outliers, and outliers are plotted individually. Timeseries of b) water year (October–September) averaged streamflow, (c) December–January–February–March–April–May (DJFMAM) streamflow and (d) August–September (AS) streamflow. The thick line shows the ten-year running average. The dashed black line indicates the mean for the time period.

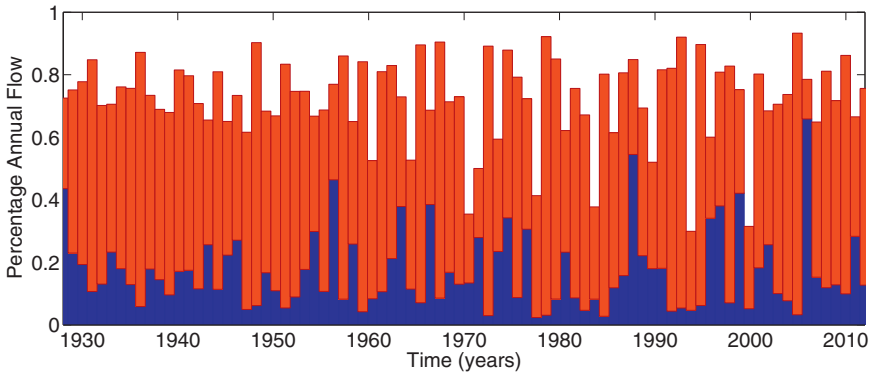

Fig. 3. DJFMAM (red bars) and AS (blue bars) streamflow as a percentage of total annual water year mean flow for 1928–2012. Percentage values are stacked.

averaged over the water year (October to September) (Fig. 2(b)), winter–spring (DJFMAM) (Fig. 2(c)) and summer months (AS) (Fig. 2(d)). The timeseries for water year flow (Fig. 2(b)) indicate a high flow period from about 1975 to about 1990, and low flow from about 1945 to about 1960. In addition there is substantial interannual variability in monthly flow throughout the record. There is also a large degree of variability on an annual timescale shown in the box plot of Fig. 2(a). DJFMAM flow is greater than AS flow, comprising approximately 61% of the total mean annual flow compared to 15% over the time period 1928–2012. However, certain years exist where the AS flow exhibits sharp spikes which far exceed the DJFMAM flow, notably 1988 and 2006 in which AS flow accounts for 55

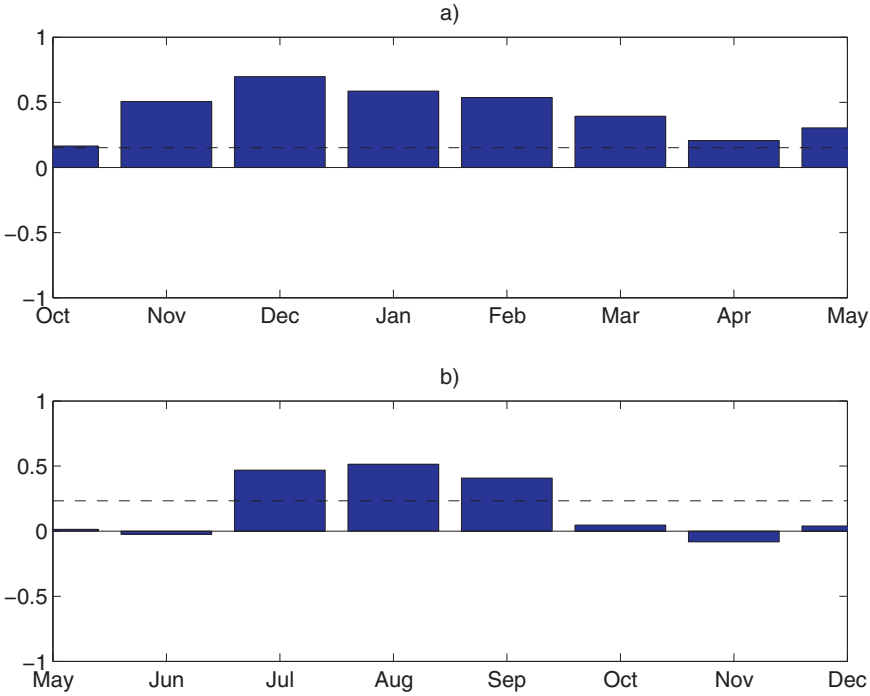

Fig. 4. Cross-correlation for (a) DJFMAM log-transformed streamflow and (b) AS log-transformed streamflow with monthly PRISM precipitation for time period of 1928–2012. Dashed line indicates significant at 0.05 level.

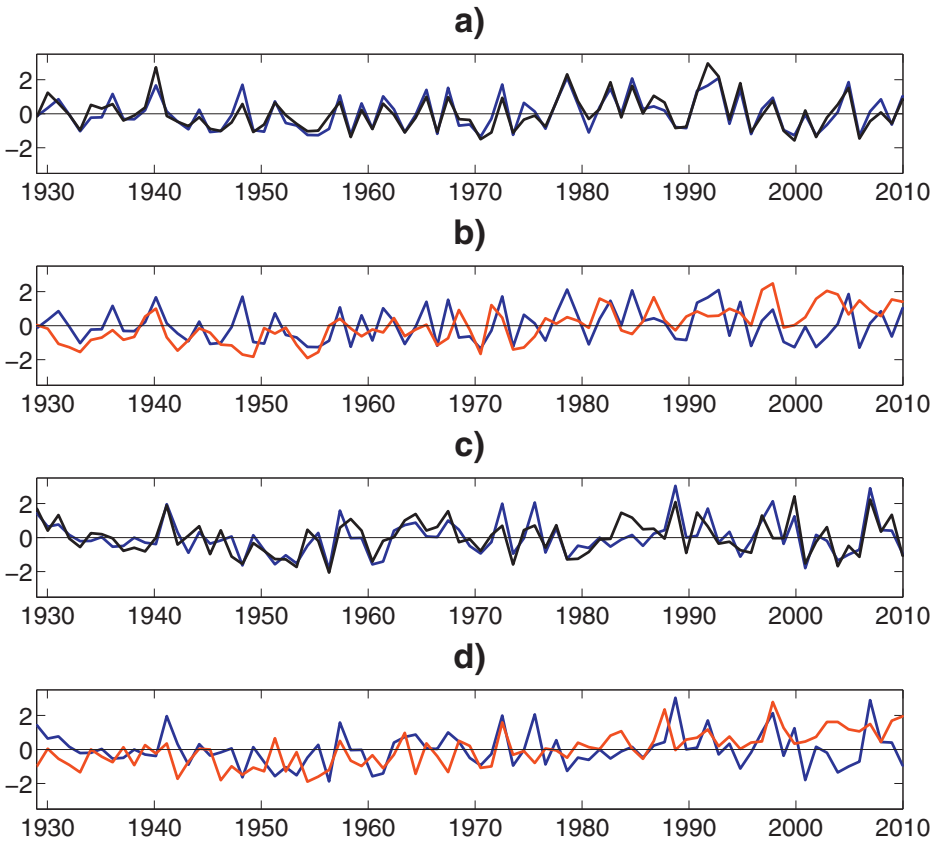

Fig. 5. Timeseries of (a) DJFMAM log-transformed streamflow and NDJFMAM PRISM precipitation, (b) DJFMAM log-transformed streamflow and Niño-4 index for NDJF, (c) AS log-transformed streamflow and JAS PRISM precipitation, and (d) AS log-transformed streamflow and Niño-4 index for JAS. The data are averaged by year and standardized for time period of 1928–2012.

and 66% of the annual mean flow respectively (Fig. 3). The mean cumulative flow was found to be 140 million cubic meters per year, with a maximum mean flow rate of 13 c.m.s. (occurring in December), and a minimum mean flow rate of 1.2 c.m.s. (occurring in June).

As can be seen in Fig. 2 the distributions of winter–spring and summer flow are positively skewed, and for this reason subsequent analysis is performed using log-transformed flow data. This improves the value of the correlations since the flow data does not vary linearly with precipitation and other variables (for example see Gutzler (2013)). The timeseries for log-transformed DJFMAM and AS streamflow over the time period 1928 to 2012 were then cross-correlated (using Pearson correlation) with PRISM precipitation, first by month and then by season (Fig. 4). For the monthly analysis, DJFMAM streamflow was found to correlate best with the concurrent winters precipitation, obtaining a maximum correlation coefficient in December of r=0.70 (p< 0.000) (Fig. 4(a)). The lag of flow behind precipitation is consistent with winter precipitation falling as snow and being stored in the basin until spring snowmelt. The seasonal correlation between DJFMAM log-transformed streamflow and winter average (NDJFMAM) precipitation is even higher with a value of r=0.91 (p< 0.000). For monthly analysis of AS log-transformed streamflow, the highest correlation with precipitation is found for the preceding and coincident months of July–August–September (JAS) reaching a maximum value of r=0.52 (p< 0.000) in August (Fig. 5(b)). The seasonal correlation coefficient between JAS precipitation and AS log-transformed flow gave a value of r=0.77 (p<0.000). The lack of any lag between precipitation and flow is because summer precipitation falls as rain with little storage in the basin. Timeseries for

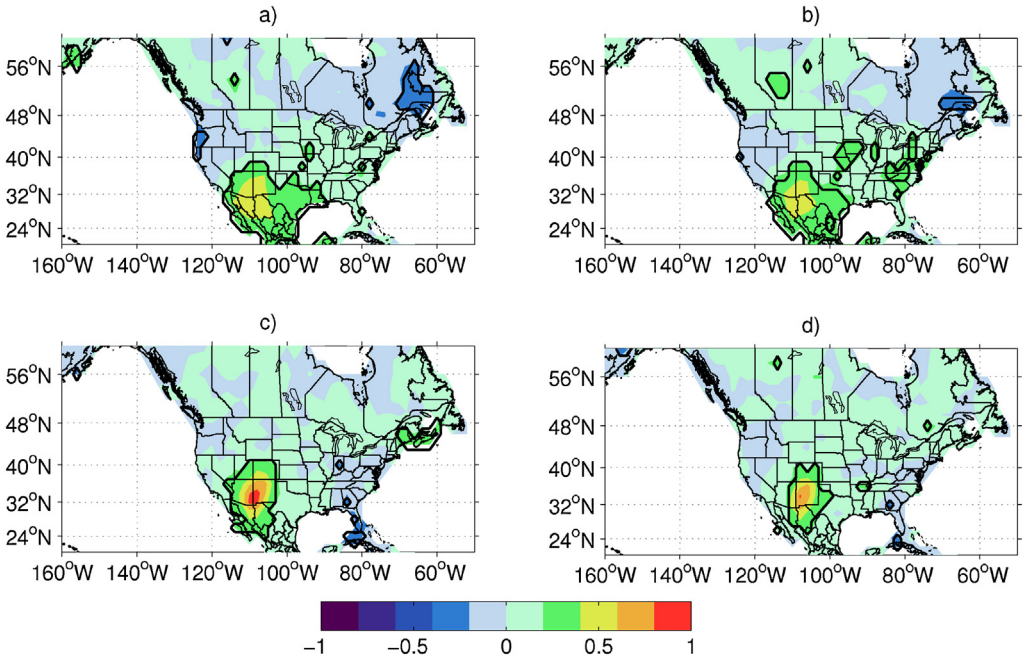

Fig. 6. Correlation of North American GPCC precipitation for winter–spring (NDJFMAM) with (a) PRISM NDJFMAM precipitation for the Upper Gila Hydrological Unit and (b) log-transformed winter–spring (DJFMAM) streamflow and for summer (JAS) with (c) PRISM JAS precipitation and (d) log-transformed summer (AS) flow. Areas that are significant at $p<0.05$ lie within the black contour.

DJFMAM log-transformed flow with NDJFMAM PRISM precipitation and NDJF SST anomalies in the Niño 4 region for 1928–2012 show the coupling of winter–spring flow with both precipitation and Pacific Ocean SST anomalies (Fig. 5(a and b)). A 7-year running average was applied to both time series (not shown) to investigate lower frequency Pacific SST impact on streamflow. This produces a positive correlation of $r=0.45$ ($p<0.000$) with explained variance of 20% ($r^2=0.20$). The relationship of decadal smoothed winter streamflow with the Pacific Decadal Oscillation index (not shown) also indicates a positive correlation between the two ($r=0.59$, $p<0.00$). In addition, 35% of the variance is explained by the relationship between PDO and streamflow ($r^2=0.35$).

The weaker correspondence of AS log-transformed flow with JAS precipitation and Niño-4 SST anomalies is also demonstrated (Fig. 5(c and d). While the summer (AS) season correlation between Gila streamflow and basin precipitation is still quite high ($r^2=0.52$, $p<0.000$), it is lower than in winter. To explain this the relationship of summer flow with evapotranspiration and temperature from the GLDAS CLM and VIC models and the NCEP-NCAR reanalysis averaged over the Gila River Basin (spanning 108.5–111.5 W and 31.5–33.5 N) was also investigated. Results from these studies (not shown) indicate weak correlations between AS summer flow and evaporation, temperature and precipitation – evaporation. Weak correlation is also found to exist between these variables amongst the different models and datasets which calls into question the validity of the evapotranspiration data. An additional analysis for the longer time period July–August–September–October–November as well as considering data for a smaller area corresponding to the watershed, were also performed to capture all basin storage but this did not improve the correlations.

PRISM precipitation for the Upper Gila Hydrological Unit in NDJFMAM as well as log-transformed DJFMAM streamflow is correlated with GPCC precipitation over North America (Fig. 6(a) and (b)). The largest correlation coefficients (aside from the region directly over or adjacent to the Gila River basin) are found to occur across all of southwestern North America including the southern (values of approximately 0.5) and central Plains (also with a value of approximately 0.5). Negative correlation

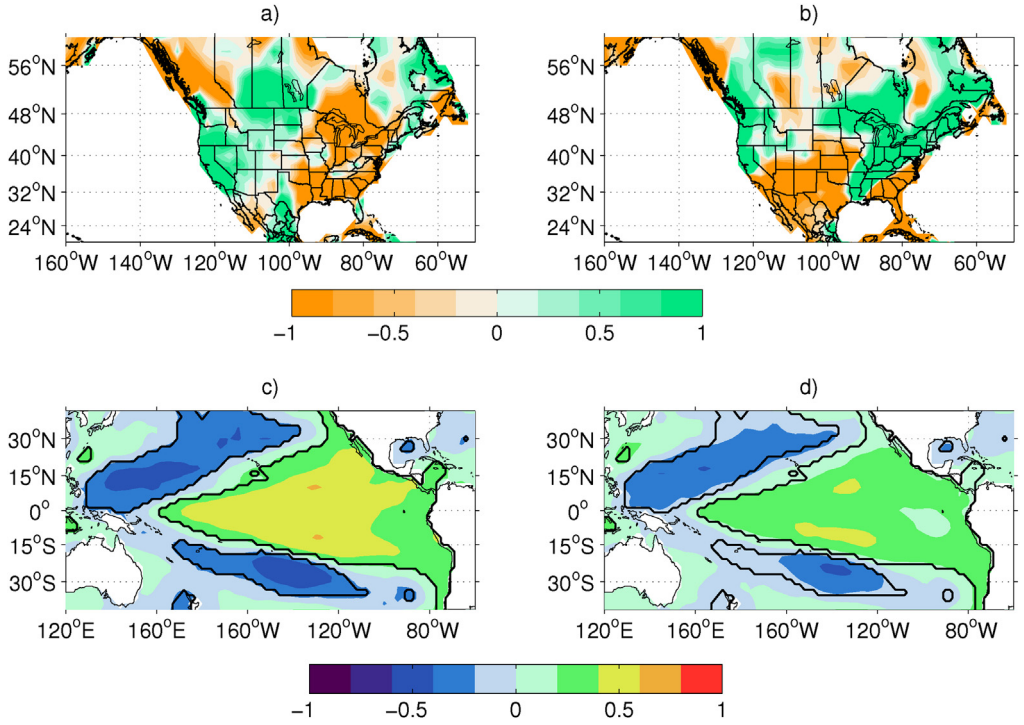

Fig. 7. Composites for North American NDJFMAM GPCC precipitation (mm/month) for (a) anomalously warm years and (b) anomalously cold years in the Nino-4 region (150°W to 160°E and 5°N to 5°S). Warm (cold) years identified by years in which value of the Nino-3.4 index for the DJF season has an anomaly greater (less) than 0.5°C. Correlation of (c) NDJFMAM PRISM precipitation over Gila River basin with DJFMAM SST and d) DJFMAM streamflow with DJFMAM SST. Areas that are significant at $p<0.05$ lie within the black contour.

coefficients stretch inland from the Pacific Northwest. This pattern of positive and negative correlations is a typical ENSO pattern (Ropelewski and Halpert, 1986, 1989, 1996). The JAS PRISM precipitation and the log-transformed AS streamflow is correlated with JAS GPCC precipitation over the region of Gila River watershed (Fig. 6(c) and (d)). These maps demonstrate the localized nature of summer flow which is consistent with local-scale convective precipitation.

Streamflow during the peak months, and PRISM precipitation for the preceding NDJFMAM and JAS, were then correlated with global SST anomalies for JFM and JAS, respectively (Fig. 7(c) and (d)). This is based on the assumption that there should be little lag between SST anomalies and the resulting atmospheric circulation anomalies that cause precipitation anomalies. The results show a positive correlation with SSTs in the ENSO region for DJFMAM streamflow and NDJFMAM precipitation with correlation coefficients reaching approximately 0.5. The greatest correlation coefficients appear to occur in the Niño-4 region. The SST correlation pattern extends from the west coast of South America to about the dateline, with cool waters to the north and south in the classic boomerang shape, all features typical of ENSO warm phase anomalies (Trenberth, 1997). A similar southwestern North American precipitation response to tropical SST has been documented in previous studies (Wu et al., 2009; Dai, 2013). Composites of North American precipitation during NDJFMAM for years of warm and cold SST anomalies in the Niño-4 regions are shown in Fig. 6(a) and (b). During anomalously warm years in the Niño-4 region, positive precipitation anomalies occur over southern North America and Mexico. Negative precipitation anomalies are found over the Southwest region corresponding to the Gila River basin during anomalously cold years.

Years of high streamflow are defined as years in which the streamflow value in DJFMAM flow is 85% or greater than the annual mean flow (4 events identified), or less than 15% for low flow years

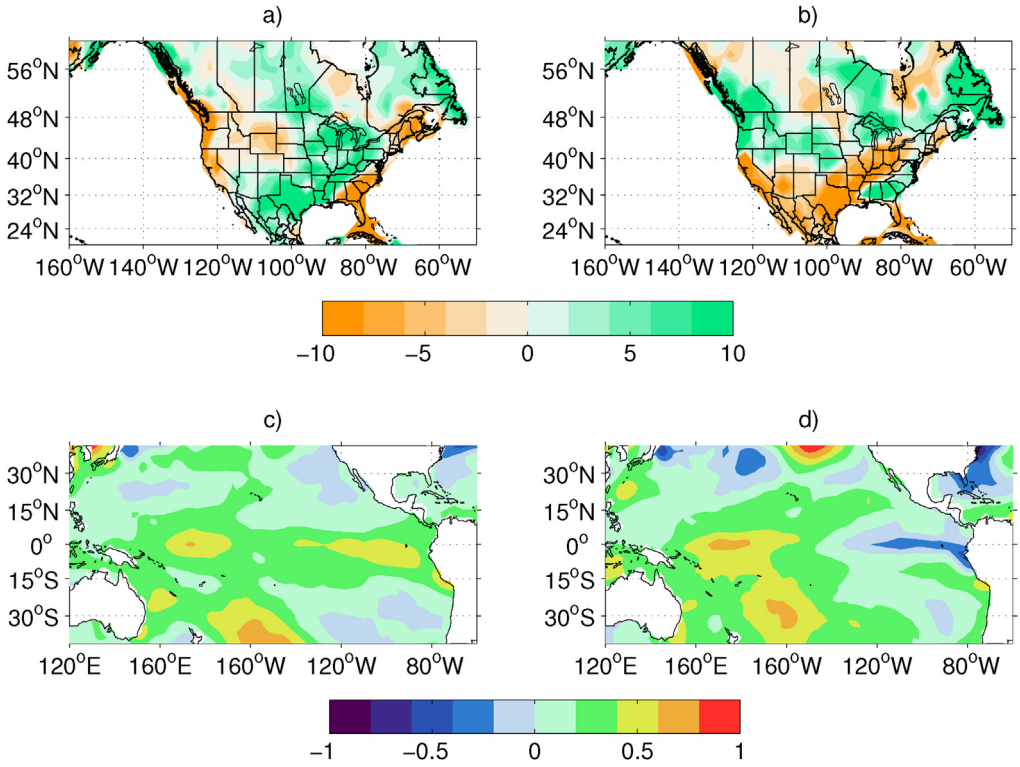

Fig. 8. Climate composites for periods of high and low streamflow, defined as high flow for years in which DJFMAM streamflow is greater than 85% of the annual flow, and low flows when 15% or less for 1928–2012. High streamflow composite for (a) NDJFMAM GPCC precipitation anomaly and (c) DJFMAM SST anomaly, and low streamflow composite for (b) NDJFMAM GPCC precipitation anomaly and (d) DJFMAM SST anomaly.

(3 events identified) over 1928–2012. Fig. 8(a) illustrates a GPCC precipitation composite for the high streamflow years. This demonstrates negative precipitation anomalies over the West and East coast. Positive anomalies exist over the Plains region, the Gulf and over Mexico. This pattern of precipitation anomalies is similar to that expected during an ENSO warm phase (Ropelewski and Halpert, 1986). A composite of JFM SST anomalies (Fig. 8(c)) for these high streamflow years shows weak warm anomalies in the central tropical Pacific region. This resembles El Niño conditions but the pattern in the eastern tropical Pacific is not typically El Niño-like in that there are cool off-equatorial SST anomalies. The low streamflow years have below normal precipitation anomalies (Fig. 8(b)) over southwest North America and above normal on the northwest coast of the United States. The SST anomalies for the low flow composite are La Niña like. It is noted that La Niña conditions exert a less strong influence on winter–spring streamflow. This is consistent with prior work that the connection between ENSO and southwest precipitation is nonlinear with El Niño exerting a stronger influence than La Niña as in Zhang et al. Zhang et al. (2014) and references therein.

Decadal variability is investigated in Fig. 9, with years of high streamflow taken as 1977–1997 (after the 1977 climatic shift in the Pacific) (Fig. 9b,e), and low streamflow as 1945–1960 (Fig. 9(a) and (d)). These different time periods for high and low flow are selected based on analysis of the 10-year running mean of the timeseries for Gila River streamflow from 1928 to 2012 in Fig. 2(b)–(d). Decadal trends are particularly apparent in the annual average for streamflow shown in Fig. 2(b), with a mean value of 6 c.m.s. occurring for the years 1977–1997 and 3 c.m.s. for the low flow years of 1945–1960. The most recent period, 1999–2012, is also investigated (Fig. 9(c) and (f)). During the high streamflow period (Fig. 9a,d) positive precipitation anomalies are observed over southwestern North America and

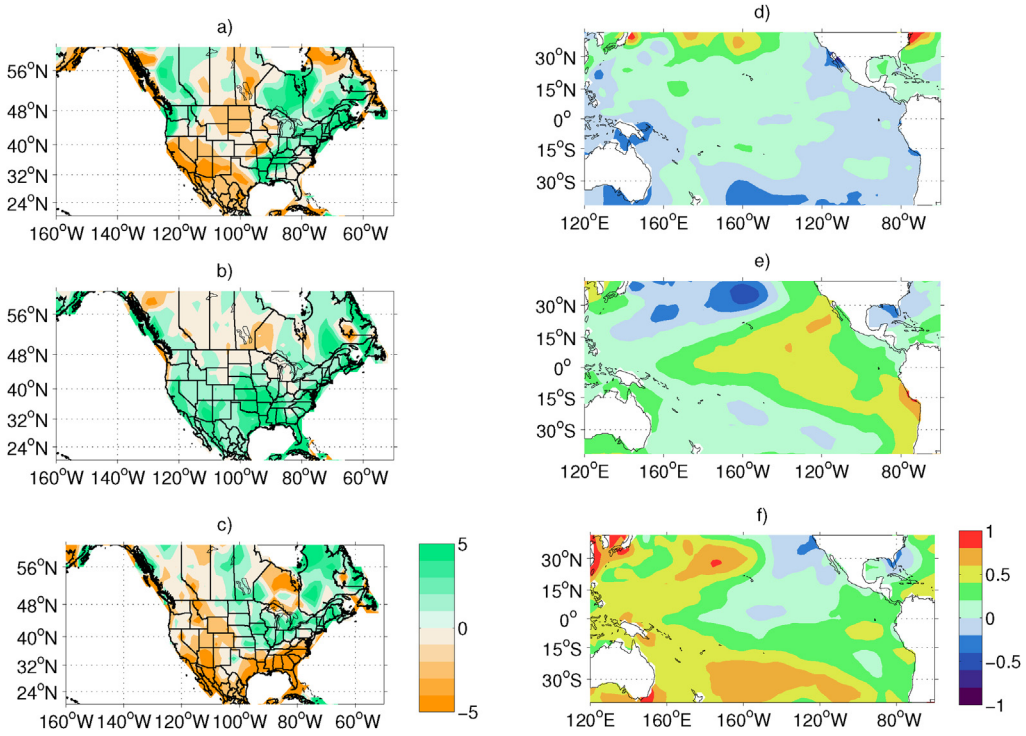

Fig. 9. Composite for North American GPCC precipitation during (a) 1945-60 period of generally lower flows, (b) 1977–1997 period of generally higher flows and (c) for the most recent decade 1999–2012 for NDJFMAM. Composites for SST anomalies during (d) 1945–1960 period of generally lower flows, (e) 1977–1997 period of generally higher flows and (f) for the most recent decade 1999–2012 for DJFMAM over the Pacific.

the Gulf Region. This pattern again resembles the El Niño related precipitation anomaly pattern over North America. Consistently, positive SST anomalies occur in the central and eastern Pacific within a meridionally broad pattern resembling decadal El Niño variability (Zhang et al., 2012). A region of negative SST anomalies is also found to occur in the North Atlantic region. For the low streamflow years (Fig. 9(b) and (e)) negative precipitation anomalies occur over southwest North America, the coastal southeast U.S. and the Gulf region. Positive anomalies occur over the northwest and much of the eastern U.S. However the SST anomalies in the Pacific and Atlantic Oceans do not clearly show any climate mode pattern. The most recent decade (Fig. 9(c) and (f)) shows positive precipitation anomalies over the north west United States, and negative anomalies over the south west and Gulf Region. Pacific Ocean SST has generally warm anomalies in the tropics but cold anomalies in the central Pacific. Consistently it has been shown using SST-forced atmosphere models how a shift in the late 1990s to this SST pattern induced drying across southwest North America (Hoerling et al., 2009; Seager and Vecchi, 2010).

The Upper Gila Watershed is surrounded by a dense network of moisture sensitive tree-ring chronologies that offer a high-quality and long-term perspective on moisture variability in the centuries prior to the instrumental era. The June–August PDSI reconstruction from the North American Drought Atlas (Cook et al., 2010); Fig. 10(b)) illustrates that in the Upper Gila Basin, persistent pluvials centered on the 1910s and 1980s, made the 20th Century perhaps the wettest of the last millenium. It also highlights protracted drought events previously described in the late 16th century (e.g. (Stahle et al., 2009)), and several “megadroughts” of the late Medieval Era (e.g., (Meko et al., 2007; Cook et al., 2007; Williams et al., 2013)). The anomalously wet 20th century, 16th century “megadrought,” and another multidecadal drought event in the early 1400s are also evident in an

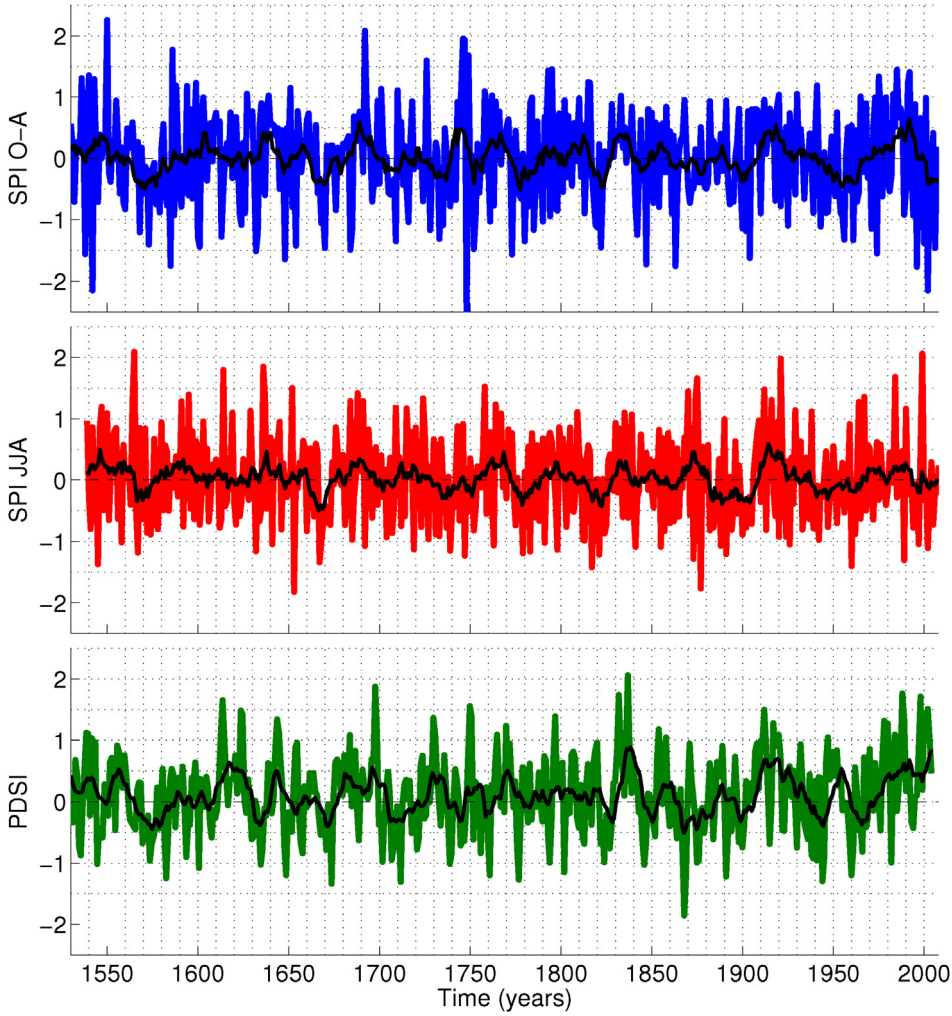

Fig. 10. Top time series: reconstructed Standardized Precipitation Index (SPI) (blue line) for 7 months from October to April for 1530 to 2008. Middle time series: Reconstructed SPI (red line) for 2 months from July to August for 1539–2008. Bottom time series: Reconstructed PDSI from treering data (green line) from 1530 to 2003. The data are derived from the region of the Gila River drainage basin. The original annual data are smoothed using a moving average over a 10 year interval.

unpublished reconstruction of water year flow on the Gila River downstream at Safford Arizona, which covers the period 1332–2005 A.D. [Meko and Hirschboeck, http://treeflow.info/loco/gila.html].

A novel perspective on paleomonsoon precipitation variability in this region is available from summer-forming tree-ring "latewood" (Griffin et al., 2011). Latewood chronologies have been used to reconstruct June–August standardized precipitation indices for a large area of Arizona and western New Mexico (Griffin et al., 2013). In the Southwestern U.S., precipitation influence on the summer PDSI is dominated by the cool season (George et al., 2010) and for data in the present study, the relationship between summer PDSI with previous NDJFMAM PRISM precipitation (r=0.42, p<0.000) is greater than that with the monsoon (JAS) precipitation (not significant). The summer PDSI is also found to correlate greater with the winter–spring SPI index over 1530–2003 (r=0.47, p<0.000) than with the summer SPI (not significant). The SPI demonstrates synchronous periods of negative SPI index between the winter–spring (October–April) and summer around 1575, 1675, 1775, 1825, 1880, and

1950 among other periods (although in general the correlation between the two is insignificant). This supports recent Southwestern studies using latewood which find that major decadal droughts of the last several centuries were likely characterized by precipitation deficits during both seasons (Stahle et al., 2009; Faulstich et al., 2013; Woodhouse et al., 2013; Griffin et al., 2013).

4. Conclusion

We have presented the first comprehensive analysis of the climatic causes of Gila River flow variability over the time period 1928–2012. The Gila River experiences two peaks in its hydrograph: one in the winter to spring (DJFMAM) with a monthly mean magnitude of approximately 5.6 c.m.s., and a second, smaller, peak (about 2.7 c.m.s.) in the summer (AS) coinciding with the North American Monsoon The DJFMAM streamflow peak correlates the greatest with precipitation in the preceding NDJFMAM months, with the delay being consistent with winter precipitation falling as snow in the headwaters and moving into the river in spring following snowmelt. The AS streamflow peak correlates the greatest, but at a lower value, with JAS precipitation, the lack of any appreciable lag being consistent with Monsoon precipitation falling as rain and moving quickly into the river. Correlation and composite analyses show that DJFMAM streamflow and NDJFMAM precipitation are positively related to an ENSO like pattern of Pacific SST anomalies. These relations hold in general for individual year examples of high and low spring flows. In contrast, AS streamflow and precipitation does not have an association to Pacific SST. The weaker link between AS streamflow and summer precipitation, and between summer precipitation and SST anomalies, indicates future studies are needed focused on North American Monsoon variability and the role of other controls on streamflow such as temperature and evapotranspiration variability. In addition the Gila River basin is affected by highly localized climate variability involving the monsoon and convective storms, particularly during the summer months, which may be more difficult to quantify by rain gauges and requires analysis to be performed at the mesoscale.

The Gila River flow also has impressive variability on decadal timescales. This can be explained in large part by decadal ENSO-like variability with the composite for the high flow decades of 1975 to 1990 clearly revealing the warm phase of Pacific decadal variability. The post 1990s decline in Gila River flow is also explained in terms of the shift to cooler tropical Pacific SSTs. The reconstructed PDSI and SPI indexes for past centuries demonstrate prolonged droughts and pluvials as well as periods of synchronous summer and winter dry periods.

The history of the spring maxima of Gila River flow can therefore be largely explained in terms of natural precipitation variability forced by interannual to decadal ENSO variability. This should allow some useful seasonal to interannual predictabilty of spring Gila River flows. The high flows in the late 20th Century are associated with the warm phase of Pacific decadal variability and the recent downturn in the 21st Century is consistent with the more generally cold tropical Pacific conditions since the 1997/1998 El Niño. As the current century evolves, Gila River flow will no doubt be influenced by human-induced climate change but natural variability such as that identified here will also continue. Projections of future Gila River flows, and its important contribution to southwest water resources, will need to account both for the natural variability and the response to human-induced climate change.

Acknowledgments

This work was supported by NSF award AGS-1243204 and NOAA award NA10OAR4310137 “Linking near-term future changes in weather and hydroclimate in western North America to adaptation for ecosystem and water management”. LDEO contribution number XXXX. We thank Jennifer Nakamura and Naomi Henderson for invaluable help preparing the figures. We thank Andrea Ray for useful comments on the manuscript. We thank the editor and the anonymous reviewers for comments that improved the manuscript.

References

Adams, D.K., Comrie, A.C., 1997. The North American Monsoon. Bull. Am. Meteorol. Soc. 78 (10), 2197–2213, http://dx.doi.org/10.1175/1520-0477(1997)078<2197:TNAM>2.0.CO;2.

Barlow, M., Nigam, S., Berbery, E., 1998. Evolution of the North American Monsoon system. J. Clim. 11 (9), 2238–2257.
Barlow, M., Nigam, S., Berbery, E.H., 2001. ENSO, pacific decadal variability, and U.S. summertime precipitation, drought, and stream flow. J. Clim. 14 (9), 2105–2128, http://dx.doi.org/10.1175/1520-0442(2001)014<2105:EPDVAU>2.0.CO;2.
Cayan, D., Redmond, K., Riddle, L., 1999. ENSO and hydrologic extremes in the western United States (vol. 12, p. 2881, 1999). J. clim. 12 (12), 3516.
Cook, B.I., Seager, R., 2013. The response of the North American Monsoon to increased greenhouse gas forcing. J. Geophys. Res. Atmos. 118 (4), 1690–1699.
Cook, E., Lall, U., Woodhouse, C., Meko, D., 2004. North American PDSI reconstructions. NOAA Paleoclimatol.
Cook, E.R., Seager, R., Cane, M.A., Stahle, D.W., 2007. North American drought: reconstructions, causes, and consequences. Earth-Sci. Rev. 81 (1–2), 93–134.
Cook, E.R., Seager, R., Heim, R.R., Vose, R.S., Herweijer, C., 2010. Megadroughts in North America: placing IPCC projections of hydroclimatic change in a long-term palaeoclimate context. J. Quat. Sci. 25 (1), 48–61.
Dai, A., 2013. The influence of the inter-decadal Pacific oscillation on U.S. precipitation during 1923–2010. Clim. Dyn. 41 (3–4), 633–646.
Daly, C., Halbleib, M., Smith, J.I., Gibson, W.P., Doggett, M.K., 2008. Physiographically sensitive mapping of climatological temperature and precipitation across the conterminous united states. Int. J. Clim. 28 (15), 2031–2064.
Faulstich, H.L., Woodhouse, C.A., Griffin, D., 2013. Reconstructed cool- and warm-season precipitation over the tribal lands of northeastern Arizona. Clim. Change 118 (2), 457–468.
Gebremichael, M., Vivoni, E.R., Watts, C.J., Rodriguez, J.C., 2007. Submesoscale spatiotemporal variability of North American Monsoon rainfall over complex terrain. J. Clim. 20 (9), 1751–1773.
Griffin, D., Meko, D.M., Touchan, R., Leavitt, S.W., Woodhouse, C.A., 2011. Late chronology development for summer moisture reconstruction in the U.S. Southwest. Tree-Ring Res. 67 (2), 87–101.
Griffin, D., Woodhouse, C.A., Meko, D.M., Stahle, D.W., Faulstich, H.L., 2013. North American Monsoon precipitation reconstructed from tree-ring latewood. Geophys. Res. Lett. 40 (5), 954–958.
Gutzler, D.S., 2013. Streamflow Projections for the Upper Gila River. New Mexico Interstate Stream Commission.
Gutzler, D.S., Kann, D., Thornbrugh, C., 2002. Modulation of ENSO-based long-lead outlooks of southwestern U.S. winter precipitation by the pacific decadal oscillation. Weather Forecast. 17 (6), 1163–1172.
Hoerling, M., Quan, X.-W., Eischeid, J., 2009. Distinct causes for two principal U.S. droughts of the 20th century. Geophys. Res. Lett. 36 (19).
Hurd, B.H., Coonrod, J., 2008. Climate change and its implications for New Mexico's water resources and economic opportunities. New Mexico State University, Agricultural Experiment Station, Cooperative Extension Service, College of Agriculture and Home Economics.
Kahya, E., Dracup, J.A., 1993. U.S. streamflow patterns in relation to the el ni no/southern oscillation. Water Resour. Res. 29 (8), 2491–2503.
Kahya, E., Dracup, J.A., 1994. The influences of type 1 el nino and la nina events on streamflows in the pacific southwest of the United States. J. Clim. 7 (6), 965–976.
Kalnay, E., Kanamitsu, M., Kistler, R., Collins, W., Deaven, D., 1996. The NCEP/NCAR 40-year reanalysis project. Bull. Am. Meteorol. Soc. 77 (3), 437–471.
Liang, X., 1994. A Two-layer Variable Infiltration Capacity Land Surface Representation for General Circulation Models. University of Washington (Ph.D. thesis).
Liverman, D., Merideth, R., 2002. Climate and society in the US Southwest: the context for a regional assessment. Clim. Res. 21 (3), 199–218.
McCabe, G., Palecki, M., Betancourt, J., 2004. Pacific and Atlantic Ocean influences on multidecadal drought frequency in the United States. Proc. Natl. Acad. Sci. 101 (12), 4136–4141.
Meko, D.M., Baisan, C.H., 2001. Pilot study of latewood-width of conifers as an indicator of variability of summer rainfall in the North American Monsoon region. Int. J. Clim. 21 (6), 697–708.
Meko, D.M., Woodhouse, C.A., Baisan, C.A., Knight, T., Lukas, J.J., Hughes, M.K., Salzer, M.W., 2007. Medieval drought in the upper Colorado river basin. Geophys. Res. Lett. 34 (10).
Molles, M.C., Dahm, C., 1990. A perspective on El Niño and La Niña: global implications for stream ecology. J. N. Am. Benthol. Soc. 9 (1), 68–76.
Notaro, M., Liu, Z., Gallimore, R.G., Williams, J.W., Gutzler, D.S., Collins, S., 2010. Complex seasonal cycle of ecohydrology in the southwest united states. J. Geophys. Res. Biogeosci. 115 (G4), http://dx.doi.org/10.1029/2010JG001382.
Redmond, K.T., Koch, R.W., 1991. Surface climate and streamflow variability in the western United States and their relationship to large-scale circulation indices. Water Resour. Res. 27 (9), 2381–2399, http://dx.doi.org/10.1029/91WR00690.
Rodell, M., Houser, P., Jambor, U., Gottschalck, J., Mitchell, 2004. The global land data assimilation system. Bull. Am. Meteorol. Soc. 85 (3), 381–394.
Ropelewski, C.F., Halpert, M., 1996. Quantifying southern oscillation–precipitation relationships. J. Clim. 9 (5), 1043–1059.
Ropelewski, C.F., Halpert, M.S., 1986. North American precipitation and temperature patterns associated with the El Niño/Southern oscillation (ENSO). Mon. Weather Rev. 114 (12), 2352–2362.
Ropelewski, C.F., Halpert, M.S., 1989. Precipitation patterns associated with the high index phase of the southern oscillation. J. Clim. 2 (3), 268–284.
Schubert, S.D., Suarez, M., Pegion, P., Koster, R., Bacmeister, J., 2004. On the cause of the 1930 dust bowl. Science 303 (5665), 1855–1859.
Seager, R., Goddard, L., Nakamura, J., Henderson, N., Lee, D.E., 2014. Dynamical causes of the 2010/11 Texas-Northern Mexico drought*. J. Hydrometeorol. 15 (1), 39–68.
Seager, R., Harnik, N., Robinson, W., Kushnir, Y., Ting, M., 2005a. Mechanisms of ENSO-forcing of hemispherically symmetric precipitation variability. Q. J. R. Meteorol. Soc. 131 (608), 1501–1527.
Seager, R., Kushnir, Y., Herweijer, C., Naik, N., Velez, J., 2005b. Modeling of tropical forcing of persistent droughts and pluvials over Western North America: 1856–2000. J. Clim. 18 (19), 4065–4088.

Seager, R., Ting, M., Held, I., Kushnir, Y., Lu, J., 2007. Model projections of an imminent transition to a more arid climate in southwestern North America. Science 316 (5828), 1181–1184.
Seager, R., Vecchi, G.A., 2010. Greenhouse warming and the 21st century hydroclimate of southwestern North America. Proc. Natl. Acad. Sci. U.S.A. 107 (50), 21277–21282.
Seth, A., Rauscher, S.A., Biasutti, M., Giannini, A., Camargo, S.J., 2013. Cmip5 projected changes in the annual cycle of precipitation in monsoon regions. J. Clim. 26 (19), 7328–7351.
Sheppard, P., Comrie, A., Packin, G., Angersbach, K., Hughes, M., 2002. The climate of the U.S. Southwest. Clim. Res. 21 (3), 219–238.
Smith, T.M., Reynolds, R.W., Peterson, T.C., Lawrimore, J., 2008. Improvements to NOAA's historical merged land–ocean surface temperature analysis (1880–2006). J. Clim. 21 (10), 2283–2296.
St. George, S., Meko, D.M., Cook, E.R., 2010. The seasonality of precipitation signals embedded within the North American drought atlas. Holocene 20 (6), 983–988.
Stahle, D.W., Cleaveland, M.K., Grissino-Mayer, H.D., Griffin, R.D., Fye, F.K., 2009. Cool- and warm-season precipitation reconstructions over Western New Mexico. J. Clim. 22 (13), 3729–3750.
Trenberth, K.E., 1997. The definition of El Niño. Bull. Am. Meteorol. Soc. 78 (12), 2771–2777.
Williams, A.P., Allen, C.D., Macalady, A.K., Griffin, D., Woodhouse, C.A., Meko, D.M., Swetnam, T.W., Rauscher, S.A., Seager, R., Grissino-Mayer, H.D., et al., 2013. Temperature as a potent driver of regional forest drought stress and tree mortality. Nat. Clim. Change 3 (3), 292–297.
Woodhouse, C.A., Meko, D.M., Griffin, D., Castro, C.L., 2013. Tree rings and multiseason drought variability in the lower Rio Grande Basin. Water Resour. Res. 49 (2), 844–850.
Wu, B., Zhou, T., Li, T., 2009. Contrast of rainfall–SST relationships in the western north pacific between the ENSO-developing and ENSO-decaying summers. J. Clim. 22 (16), 4398–4405.
Zhang, T., Perlwitz, J., Hoerling, M.P., 2014. What is responsible for the strong observed asymmetry in teleconnections between El Niño and La Niña. Geophys. Res. Lett. 41 (3), http://dx.doi.org/10.1002/2013GL058964, 2013GL058964.
Zhang, Y., Qian, Y., Duliere, V., Salathe, E.P., Leung, L.R., 2012. ENSO anomalies over the Western United States: present and future patterns in regional climate simulations. Clim. Change 110 (1–2), 315–346.